Aggregation Mechanisms of Cystatins: A Comparative Study of Monellin and Oryzacystatin

ARTICLE *in* BIOCHEMISTRY · MARCH 2010

Impact Factor: 3.02 · DOI: 10.1021/bi902039s · Source: PubMed

7 AUTHORS, INCLUDING:

Kris Pauwels
Vrije Universiteit Brussel
24 PUBLICATIONS **250** CITATIONS
SEE PROFILE

Piero Andrea Temussi
MRC National Institute for Medical Research
222 PUBLICATIONS **4,768** CITATIONS
SEE PROFILE

BIOCHEMISTRY
including biophysical chemistry & molecular biology
Article

Biochemistry **XXXX,** *XXX,* 000–000 A
DOI: 10.1021/bi902039s

Aggregation Mechanisms of Cystatins: A Comparative Study of Monellin and Orzacystatin†

Veronica Esposito,‡ Fulvio Guglielmi,§ Stephen R. Martin,‡ Kris Pauwels,‡ Annalisa Pastore,‡ Renata Piccoli,§,∥ and Piero A. Temussi*,‡,⊥

‡*MRC National Institute for Medical Research, The Ridgeway, London NW7 1AA, U.K.,* §*Department of Structural and Functional Biology, University of Naples "Federico II", School of Biotechnology, Naples, Italy,* ∥*Istituto Nazionale di Biostrutture e Biosistemi (INBB), Naples, Italy, and* ⊥*Department of Chemistry, University of Naples "Federico II", Naples, Italy*

Received November 30, 2009; Revised Manuscript Received February 26, 2010

ABSTRACT: Identification of diseases caused by protein misfolding has increased interest in the way proteins adopt non-native conformations and form aggregates. In this study we address the question of how proteins sharing the same fold respond to destabilizing environmental conditions. We have studied the behavior of two members of the cystatin superfamily, MNEI, a single chain monellin, and oryzacystatin_I, a plant cystatin. Despite the close similarity of their three-dimensional architecture, these two proteins aggregate in a different way: MNEI gives rise to amyloid aggregation whereas oryzacystatin_I yields amorphous aggregates. Mutants of oryzacystatin_I, designed to make it more similar to MNEI, generally behave like the parent protein, but a construct devoid of the disordered N- and C-terminal sequences does show a tendency to form amyloid fibers. Our results suggest that precise sequence details may be more important than the three-dimensional architecture in determining the type of aggregate formed. Oryzacystatin_I appears to be a very promising model system for further studies of protein aggregation.

An increasing number of diseases, often termed "conformational diseases", are characterized by the presence of aggregates of misfolded proteins (*1*). To understand pathogenic behavior, it is important to study the aggregation pathway in detail (*1*−*5*).

It has been suggested that the three main mechanisms for the formation of pathological aggregates are cross-β spine, end-to-end stacking, and 3D swapping (*6*). Although the cross-β spine mechanism has been observed in the formation of classical amyloid fibrils associated with the most well-known conformational diseases, e.g., Alzheimer's, Parkinson's, and Huntington's diseases, the 3D domain swapping mechanism has recently taken center stage role, being associated with other diseases, such as cystatin C amyloid angiopathy (*7*). Since cystatin aggregation has also been studied in vitro as a typical example of an amyloid-forming protein (*8*), it seems important to investigate further the behavior of cystatins.

Cystatins, a superfamily of small proteins, include not only cysteine protease inhibitors (*9*) but also several sequences with high homology to cysteine protease inhibitors (*10*). Some cystatins are involved in human amylopathies. Amyloid aggregates of human cystatin C are found, together with the amyloid Aβ peptide, in brain arteries of old people affected by cerebral amyloid angiopathy (*11*, *12*). Cystatin C is one of the few amyloidogenic proteins for which a detailed mechanism of amyloid fiber formation has been proposed. The solid state structure of wild-type cystatin C (*13*) is a very stable dimer originating from 3D domain swapping (*14*). The 3DDS[1] mechanism requires that the protein retains most of its secondary structure elements. However, it has been shown that monellin, another member of the cystatin superfamily, can undergo typical amyloid aggregation. Native monellin is composed of two noncovalently bonded chains, A and B, where chain B occupies the N-terminal position of the cystatin fold. Konno (*15*) has shown that isolated chain B can form amyloid fibers whereas chain A does not give significant amounts of aggregates. Curiously, the author found that SCM, a single chain monellin in which the C-terminal residue of chain B is covalently linked to the N-terminal residue of chain A (*16*), does not form amyloid fibers (*15*). This observation is at variance with the fact that other cystatins of comparable length, e.g., human stefins A and B, are perfectly able to form amyloid fibers (*17*).

We investigated the aggregation mechanism of cystatins using oryzacystatin_I and MNEI, a single chain monellin in which chains B and A are joined by a GlyPhe dipeptide linker. MNEI has been thoroughly characterized from structural and functional viewpoints in previous studies from our laboratory (*18*, *19*). Here we present a comparative study of MNEI, oryzacystatin_I (hereafter designated ORYZ), and some ORYZ mutants with a particular emphasis on the relationship between structure and aggregation propensity. We have characterized all proteins by CD and NMR and monitored their aggregation using thioflavin (ThT) fluorescence, gel filtration, and electron microscopy.

EXPERIMENTAL PROCEDURES

Sample Preparation. All proteins were independently cloned in a pET-derived plasmid vector as a fusion with a 6His-glutathione *S*-transferase tag with a TEV protease cleavage site. The plasmids were transformed into *Escherichia coli* BL21(DE3).

†This research was supported in part by MIUR (Italian Ministry for the Research and University) in the form of the FIRB 2003 Grant to P.A.T.

*Corresponding author. Tel: ++39081674416. Fax: ++39081674409. E-mail: temussi@unina.it.

[1]Abbreviations: 3DDS, 3D domain swapping; CD, circular dichroism; HCCAA, cystatin C amyloid angiopathy; GST, glutathione *S*-transferase; TB, "terrific broth"; IPTG, isopropyl β-D-galactopyranoside; TEM, transmission electron microscopy; ThT, thioflavin T.

The expression was carried out by growing the cells in "terrific broth". Cell cultures were grown at 37 °C with vigorous shaking to an OD_{600} of 0.6−0.8, induced with 0.5 mM isopropyl β-D-galactopyranoside, and grown for an additional 3 h before harvesting. The cell pellet was resuspended in a lysis buffer containing 0.1 mg/mL DNase I and protease inhibitors (Complete EDTA-free; Roche) and was lysed by sonication. The cell debris was removed by centrifugation. The soluble fraction was purified by affinity chromatography using Ni-NTA agarose (QIAgen). The proteins were eluted from the column and cleaved from GST by treatment with TEV protease. Gel filtration chromatography on a G-75 (Pharmacia) column was used as an additional purification step. The nature and purity of the proteins were evaluated by mass spectrometry and SDS−PAGE electrophoresis.

Far-UV CD Analyses. Far-UV CD spectra were recorded on a Jasco J-715 spectropolarimeter fitted with a cell holder thermostated by PTC 348-WI Peltier unit. Measurements were carried out using a protein concentration of 0.2 mg mL^{-1} in fused silica cuvettes of 1 mm path length (Hellma) either in 50 mM phosphate buffer at pH 7.0 or in 15 mM glycine−HCl buffer at pH 2.5 with 0.15 M NaCl. CD spectra were typically recorded with 0.2 nm resolution and were baseline corrected by subtraction of the appropriate buffer spectrum. Heat denaturation curves were acquired increasing the temperature at a rate of 2 °C/min. The intensity of the CD signal at 215 nm was monitored at 0.2 °C intervals from 20 to 90 °C. Thermal unfolding was repeated at least twice on independent protein preparations to ensure reproducibility of the results.

ThT Fluorescence Measurements. A SPEX FluoroMax fluorometer was used for measuring the ThT fluorescence emission spectra. Excitation was at 442 nm, and spectra were recorded from 455 to 600 nm. Excitation and emission slits were set at 5 and 7 mm, respectively.

Proteins (100 μM) were incubated at 86 °C in 15 mM glycine−HCl buffer, pH 2.5, with 0.15 M NaCl. ThT fluorescence emission spectra were acquired every half hour following addition of 7 μL of the incubation solution to 800 μL of the ThT containing buffer (25 mM phosphate buffer, pH 7.0, 20 μM ThT). ThT fluorescence emission spectra were acquired immediately after adding the proteins in order to avoid perturbation of the fibril structure by the pH change from 2.5 (incubation buffer) to 7.0 (ThT buffer).

Gel Filtration. A prepacked HiLoad 10/30 Superdex 75 column (Pharmacia) was equilibrated with glycine−HCl buffer (pH 2.5) and 150 mM NaCl. Albumin (66 kDa), ovalbumin (45 kDa), chymotrypsinogen A (26 kDa), and ribonuclease A (14 kDa) were used as molecular standards for mass calibration. Samples were prepared by incubating MNEI and ORYZ (100 μM) in 15 mM glycine−HCl buffer (pH 2.5) and 150 mM NaCl at 86 or 50 °C for 6 h. After centrifugation at 13000*g* for 5 min, the supernatant was loaded on the column. Each gel filtration experiment was repeated at least three times to test for reproducibility.

Transmission Electron Microscopy. Protein samples were incubated under identical conditions as described for ThT measurements. Samples of 4 μL were spotted onto freshly carbon-coated and glow-discharged copper grids, stained with 1% sodium silicotungstate (TAAB Laboratories Equipment Ltd.), and analyzed with a JEOL 1200 transmission electron microscope operating at 100 kV. Micrographs of negatively stained areas were taken at 27800× magnification on electron microscopic films (Kodak) and developed with Phenisol developer (Ilford) and Hypam fixer (Ilford) for 5 min each.

RESULTS

Thermal Stability. The thermal stability of MNEI and ORYZ was determined by CD spectroscopy at two pH values, 2.5 and 7.0. Both pH values fall well below the p*I* of MNEI, which is approximately 9.3 (*20*). The far-UV CD spectra of MNEI at pH 2.5 and 7.0 (Figure 1S_A of Supporting Information) are consistent with the high β-sheet content and the presence of a single 16-residue α-helix, as determined by the NMR structures at acidic and neutral pH (*18*, *21*). In the case of ORYZ, the chosen pH values fall below (2.5, dotted line) and above (7.0, solid line) the p*I* (4.78). The spectra indicate a substantial β-sheet but also show a clear negative maximum at 222 nm typical of α-helix ellipticity (Figure 1S_B of Supporting Information).

It is known that single chain monellins have high thermal stability and that their transition to the unfolded state is reversible, to the extent that they can be heated to temperatures close to the boiling point of water without substantial consequences for their sweet taste (*22*). Therefore, it is not surprising that, to observe aggregation, it is necessary to heat monellins at very high temperatures for extended periods (*15*, *23*). We also checked the thermal stability and reversibility for ORYZ before performing comparative studies on fiber formation. CD spectra of MNEI, at pH 2.5, in a 15 mM glycine buffer with 0.15 M NaCl, were recorded at 10 deg intervals over the range 20−90 °C. MNEI progressively unfolds into a random coil conformation as indicated by the disappearance of the negative band at 215 nm and by the appearance of a strong negative band with a maximum just below 200 nm. The transition from β-sheet to random coil at this pH can be completely reversed if the temperature is lowered back to 20 °C within a few minutes (Figure 2S_A of Supporting Information). The behavior at pH 7.0 is similar, but reversibility is somewhat impaired by the poor solubility of the protein at neutral pH (data not shown). In the case of ORYZ the temperature-induced transition from β-sheet to random coil at pH 2.5 (pH 2.5, 15 mM glycine buffer with 0.15 M sodium chloride) can also be completely reversed if the temperature is lowered back to 20 °C within a few minutes (Figure 2S_B of Supporting Information). In contrast to MNEI, the unfolding behavior at pH 7 is also reversible, possibly because of the very different isoelectric point (data not shown).

Full heat denaturation curves for MNEI and ORYZ at both pH 2.5 and pH 7.0 were acquired by monitoring the intensity of the CD signal at 215 nm over the range 20−90 °C (Figure 1). All of the curves shown in Figure 1 are consistent with a simple two-state equilibrium between folded and unfolded forms. The fraction of the protein present in the folded form at any temperature, $f_F(T)$, is a function of $\Delta G°(T)$, the Gibbs free energy of unfolding. If we assume that the difference in heat capacity between the folded and unfolded forms, ΔC_p, is temperature independent, the Gibbs free energy is given by the Gibbs−Helmholtz equation modified so that the reference temperature is the midpoint of the high temperature unfolding transition (T_m) (*24*). A nonlinear least-squares fit to the observed CD signal (*25*) allows one to determine the midpoint unfolding temperature (T_m) and the enthalpy at this temperature (ΔH_m). Because ΔC_p is poorly defined by such data, we fixed its value at 1.4 kcal mol^{-1} K in the analysis. This is a reasonable value for proteins of this size (*26*). Values of the entropy change at T_m can be obtained from the

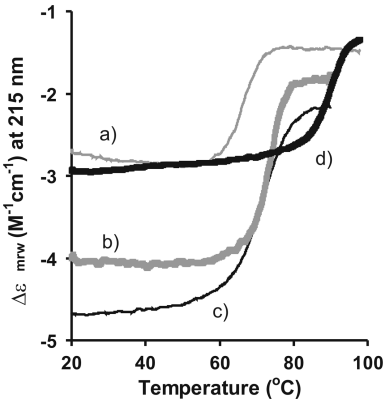

FIGURE 1: Thermal unfolding curves: (a) MNEI in glycine−HCl buffer at pH 2.5 (thin gray line); (b) MNEI in phosphate buffer at pH 7.0 (thick gray line); (c) ORYZ in glycine−HCl buffer at pH 2.5 (thin black line); (d) ORYZ in phosphate buffer at pH 7.0 (thick black line).

Table 1: Thermodynamic Parameters Derived from the Curves of Figure 1

	T_m/°C	ΔH_m/kcal mol^{-1}	ΔG^a/kcal mol^{-1}
MNEI			
pH 7.0	73.1	87.2	7.4 ± 0.8
pH 2.5	66.1	79.6	6.2 ± 0.6
ORYZ			
pH 7.0	93.5	76.2	4.4 ± 1.2
pH 2.5	71.6	55.5	2.6 ± 0.8

[a] ΔG at 20 °C calculated using the Gibbs−Helmholtz equation.

Gibbs−Helmholtz's relationship $\Delta G_m = \Delta H_m - T_m \Delta S_m$. The relevant thermodynamic parameters are summarized in Table 1. Both proteins have rather high melting temperatures (T_m), with a particularly high value for ORYZ at pH 7.0. However, the values calculated for ΔG at 20 °C indicate that MNEI is significantly more stable than ORYZ at room temperature at the pH values examined.

Aggregation. The observed decrease in the CD signal of MNEI with increasing temperature suggests partial unfolding and is consistent with the known tendency of monellin to aggregate when exposed to rather harsh environmental conditions (*15*, *23*). To verify whether the loss of signal detected in the CD spectra of MNEI could be ascribed to protein aggregation involving fibrillar structures, we monitored the effect of heating on both MNEI and ORYZ by the ThT fluorescence assay. ThT undergoes characteristic spectral changes upon binding to amyloid fibrils (*27*): an increase in the fluorescence emission intensity and a red shift of the maximum from 438 to 482 nm (*28*). We acquired ThT fluorescence emission spectra at 30 min intervals for protein samples incubated at 86 °C (see Experimental Procedures). The characteristic red shift and increase in fluorescence emission intensity were detected with MNEI samples (circles, Figure 2) but not with ORYZ (squares, Figure 2), even though the ORYZ samples do show visible signs of precipitation. The increase in ThT fluorescence emission was observed for the MNEI sample after approximately 2 h of incubation). The conclusion that MNEI forms amyloid-like fibers but ORYZ does not appears to be at variance with the observation that the ORYZ sample shows visible evidence of protein precipitation. The simplest interpretation is that ORYZ aggregates early during the incubation period as a folded protein, possibly before heating

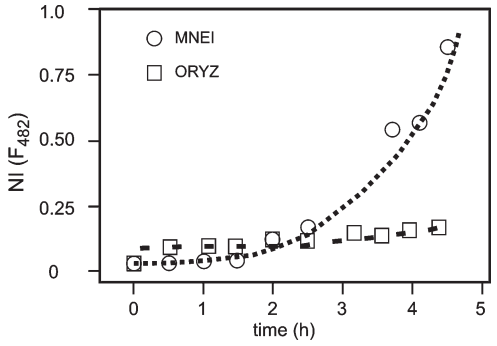

FIGURE 2: Time dependence of ThT fluorescence emission at 482 nm during protein incubation: MNEI (circles) and ORYZ (squares).

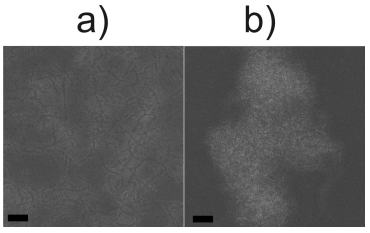

FIGURE 3: TEM analysis of MNEI and ORYZ in 15 mM glycine−HCl buffer at pH 2.5 after 3 h at 86 °C. (a) MNEI; (b) ORYZ. The black scale bars indicate 50 nm length.

can induce the conformational changes necessary to induce the formation of amyloid fibers.

Morphological characterization of aggregates of MNEI and ORYZ was performed by TEM. The differences in aggregation behavior between MNEI and ORYZ suggested by Tht fluorescence were supported by TEM experiments as different morphologies between the two samples are observed. Several incubation periods of heating were evaluated to verify reproducibility of the observations. Figure 3 shows two typical electron micrographs of the two proteins after heating for 3 h at 86 °C.

In the case of MNEI we observe individual, linear, unbranched, extended fibrils that, consistently with the ThT reactivity, strongly suggest an amyloid character. These fibrils are in agreement with the observations described by Konno (*15*) for isolated chain B of wild-type monellin.

In the case of ORYZ we observe short curved and tangled fibrils that cluster together into dense aggregate deposits. Despite extensive screening of the grids, isolated individual fibrils could not be observed, and only aggregate deposits were detected.

Size Exclusion Chromatography. The nature of this aggregation is evidenced by a size exclusion chromatography investigation. MNEI and ORYZ samples (100 μM in 15 mM glycine buffer, pH 2.5, with 0.15 M NaCl) were subjected to gel filtration chromatography before heating and then after 3 and 6 h of incubation at 86 °C. Elution profiles are shown in Figure 4. Unheated samples of MNEI elute, on a previously calibrated gel filtration column, with an elution volume consistent with a monomeric protein (Figure 4a, gray line). After 3 h (dotted black line) and 6 h (solid black line) of incubation, the only species detected was the monomer; no higher molecular weight species were eluted from the column. Nevertheless, the peak area of the monomer decreases by about 50% after 3 h of incubation and by 80% after 6 h of incubation. This indicates that the MNEI monomer disappears during the incubation and that species with higher molecular weight, which are not visible as a precipitate and

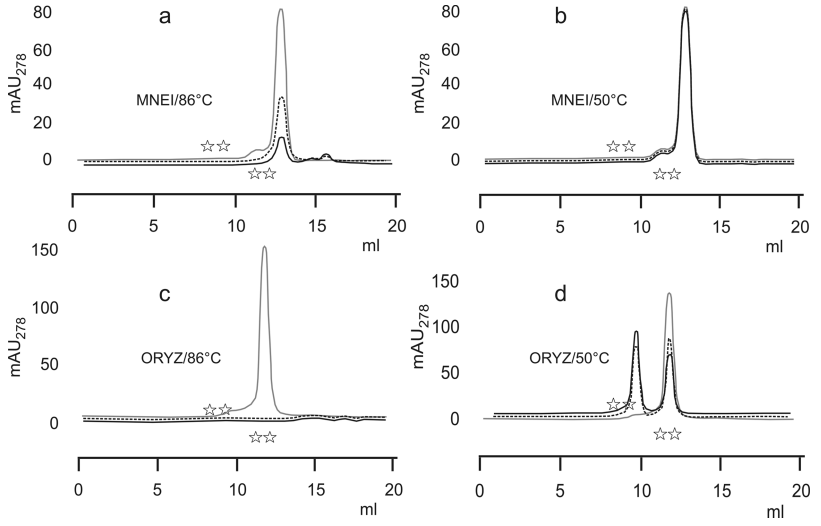

FIGURE 4: Gel filtration analysis of MNEI and ORYZ. Milliabsorption units (mAU) detected at 280 nm are plotted against retention volume. Panels a and c refer to MNEI and ORYZ, respectivel, during incubation at 86 °C. The corresponding experiments at 50 °C are shown in panels b and d for MNEI and ORYZ, respectively. Gray lines indicate the unheated proteins, dotted black lines indicate proteins incubated for 3 h, and solid black lines correspond to proteins incubated for 6 h. Asterisks (*) mark the positions of molecular mass standards, from left to right: albumin (66 kDa), ovalbumin (45 kDa), chymotrypsinogen A (26 kDa), and ribonuclease A (14 kDa).

Scheme 1:[a]

```
MNEI          GEWEIIDIG  PFTQNLGKFAVDEENKIGQYGRITFNKVIRPCMKKTIYENEGF (52)
ORYZ MSSDGGPVLGGVEPVGNENDLHLVDLARFAVTEHNKKAN SLIEFEKLVS  VKQQVVA     (56)

MNEI REIKGYEYQLYVYASDKLFRADISEDYKTRGRKLLRFNGPVPPP     (96)
ORYZ GTLYYFTIEVKEGDAKKLYEAKVWEKPWMDFKELQEFK PVDASANA (102)
```

[a]The numbers in brackets refer to residue numbers.

are not eluted from the column, are being formed. This behavior is consistent with the formation of amyloid fibers that become trapped in the gel.

Unheated samples of ORYZ also elute with an elution volume consistent with the protein being monomeric (gray line, Figure 4c). However, all protein visibly precipitates during the incubation, and no protein was detected in gel filtration analyses after 3 h (dotted black line) and 6 h (solid black line) of incubation at 86 °C.

To decrease the probability of protein precipitation, the experiments were repeated using an incubation temperature of 50 °C. After 3 h of incubation at 50 °C gel filtration of ORYZ (dotted black line in Figure 4d) reveals the presence of a second species, in addition to the monomeric protein (the area of the monomer peak after 3 h corresponds to 58% of the total population). The elution volume of the new species (42% of total) corresponds to a MW of 36 kDa (dotted black line in Figure 4d). This higher molecular weight species becomes the major one after 6 h of incubation (solid black line in Figure 4d, with an area corresponding to 56% of total). The MW of 36 kDa suggests that this species is a trimer of ORYZ, since the MW of the monomer is 11.4 kDa. The early formation of a stable oligomeric species might hinder amyloid-like aggregation for ORYZ, in agreement with the ThT assay data, because it can lead to massive aggregation of the folded protein. It is difficult, with these data, to determine whether the aggregation observed for ORYZ is simply oligomerization of the intact folded protein or is a consequence of partial unfolding followed by domain swapping. Only a direct structural study of the oligomers could yield an answer to this question, and such a study is beyond the scope of the present work. However, in order to shed more light on the mechanism of aggregation of this cystatin, we extended the stability study to a few mutants.

Mutants. In a long-standing effort for understanding the structure−taste relationships we have been attempting to design de novo sweet proteins (*29*). In one approach we designed several mutants of ORYZ, a protein structurally similar to monellin but devoid of sweet taste. The intention was to create the sweet taste by making ORYZ more similar to MNEI.

The alignment of the sequences of MNEI and ORYZ, performed with Clustal_X (*30*), is shown in Scheme 1. The N-terminal peptide of ORYZ, which contains one of the essential active sites of cysteine protease inhibitors (*31*), has no counterpart in MNEI, which probably accounts for the lack of inhibitory activity of MNEI. In addition, the NMR solution structure of ORYZ, determined by Nagata et al. (*32*), shows that the N- and C-terminal parts of the construct are completely disordered. Accordingly, most of the constructs designed to mimic MNEI lack either the nine N-terminal residues or the six C-terminal residues or both (boxed in Scheme 1).

An approach based on mutations suggested by the sequence of a cystatin of different stability is reminiscent of the chimeras between stefins A and B (*33*).

A comparison of the stability of the full-length construct with those in which these parts had been deleted confirmed that they do not contribute to the global stability of the normal fold. Most

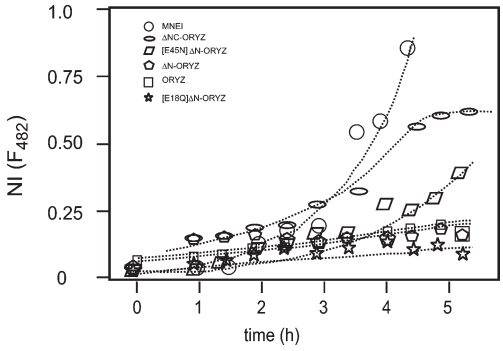

FIGURE 5: Time dependence of ThT fluorescence emission at 482 nm in the presence of different ORYZ mutants during incubation at 1 mg/mL and 86 °C in 15 mM glycine buffer, pH 2.5, with 0.15 M NaCl. Significant increases in fluorescence are only seen with ΔNC-ORYZ under the condition of this assay.

mutants were based on the construct missing the first nine N-terminal residues (ΔN-ORYZ). Two single point mutation constructs (Figure 4S of Supporting Information) were chosen because they could lead to a significant and specific destabilization of ORYZ. Mutation of Glu45 into Asn in [E45N] ΔN-ORYZ and of Glu18 into Gln in [E18Q] ΔN-ORYZ could destabilize the salt bridges of Glu45 with Lys67 and of Glu18 with Lys46.

The two potential partners of the first of these two salt bridges are on opposite sides of an interface (Figure 4S_C of Supporting Information) similar to that implicated in the domain swapping observed for cystatin C (*13*). Thus, its disruption could favor this mechanism through direct influence on the relative stability of the whole fold with respect to dissociation toward domain swapping. The other salt bridge (E18-K46) can directly influence the stability of the hydrophobic core of the protein, dominated by the interface between the helix and the β-sheet (Figure 4S_D of Supporting Information).

All mutants are correctly folded as shown by their CD and NMR spectra. Figure 3S of Supporting Information shows the comparison of 1D NMR spectra of three representative constructs: wild-type ORYZ, [E45N] ΔN-ORYZ, and [E18Q] ΔN-ORYZ.

The nature of the aggregates formed after heating these constructs was checked, as for the parent proteins, using the ThT assay. Figure 5 shows the time dependence of ThT fluorescence emission intensity at 482 nm upon incubation at 86 °C. In the case of [E45N] ΔN-ORYZ there is a modest increase after several hours of incubation. The only construct that shows a clear tendency to form amyloid fibers is ΔNC-ORYZ. These findings are consistent with the fact that the thermal stability of [E45N] ΔN-ORYZ is very similar to that of the parent protein whereas ΔNC-ORYZ has a lower melting temperature, ca. 50 °C compared with 72 °C for the parent protein (Supporting Information, Figure 5S). In spite of the fact that in the solution structure the two terminal regions appear completely disordered, the difference in thermal denaturation suggests they have some structural role. It is possible that they can effectively shield regions of the protein surface, otherwise prone to association. The fact that both regions appear completely disordered in the NMR structure may only reflect a conformational equilibrium in solution.

DISCUSSION

In this paper we have presented a comparative study of the stability and aggregation propensity of MNEI, ORYZ, and some of mutants of ORYZ. We have characterized all of the proteins

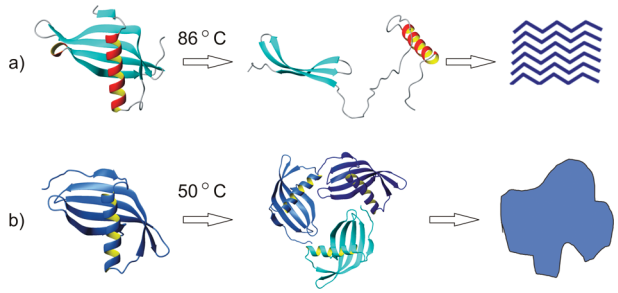

FIGURE 6: Schematic model of the two mechanisms of aggregation. (a) MNEI opens up when heated at 86 °C and then aggregates as amyloid fibers. (b) ORYZ oligomerizes when heated at 50 °C and then precipitates as an amorphous aggregate. Protein models were generated by MOLMOL (*37*).

by CD and NMR and monitored their aggregation using ThT fluorescence. Both MNEI and ORYZ are very stable with high melting temperatures. However, despite the fact that they have very similar three-dimensional architecture, MNEI and ORYZ aggregate in a different way. ThT fluorescence and TEM show that MNEI gives rise to amyloid aggregation upon incubation at high temperature whereas ORYZ yields amorphous aggregates. Gel filtration studies led to similar conclusions. MNEI samples show either monomers or high molecular weight aggregates (amyloid fibrils), whereas ORYZ, when heated at 50 °C, shows a tendency to form a stable oligomeric species corresponding to a trimer of the folded protein. The latter observation is important because early formation of oligomers of the folded protein can lead to massive aggregation when the folded protein is heated at higher temperatures. Figure 6 summarizes the two different models of aggregation of MNEI and ORYZ.

Mutants of ORYZ, designed to make it more similar to MNEI, behave in general like the parent protein; that is, they have no tendency to aggregate in amyloid fashion; only the construct devoid of the disordered N- and C-terminal sequences shows some tendency to form amyloid fibers, possibly owing to its lower thermal stability. Overall, our results suggest sequence details are more important than three-dimensional architecture in dictating the type of aggregate that will be formed upon heating.

The behavior of MNEI and ORYZ reported here is apparently not entirely consistent with the Dobson postulate (*34*), according to which virtually any protein, if properly destabilized, can aggregate in a fashion related to conformational diseases. However, it would be premature to state that the behavior of our two proteins violates the generality proposed by Dobson before a more exhaustive study at many different conditions. MNEI gives amyloid fibers whereas ORYZ gives amorphous aggregates. It would be tempting to attribute this difference to the different stability between MNEI and ORYZ, but the difference between their transition temperatures is not sufficient to attribute higher thermal stability to ORYZ. As shown by the data of Table 1, melting temperatures are very high for both proteins, with an exceptionally high value for ORYZ at pH 7.0, but the values of ΔG at 20 °C indicate a higher thermodynamic stability for MNEI in the pH range examined. In addition, we have observed that (1) ORYZ undergoes a transition at 50 °C, i.e., at a temperature much lower than T_m, and, moreover, this transition is linked to the nonamyloid transition, and (2) when the unstructured N- and C-terminal tails are cut, MNEI and ORYZ become more similar from the point of view of thermal unfolding and type of aggregation.

This last observation suggests a possible active role of the unstructured segments. It appears that either the N-terminal or the C-terminal intrinsically unfolded sequences protect ORYZ from amyloid-like aggregation. It is important to note that this is not the first observation of the role of the N-terminal in the stability of a cystatin (*35*, *36*). Last but not least, the different mechanism of aggregation of MNEI and ORYZ may be attributed to small but significant differences in their sequences.

Oryzacystatin_I appears to be a very promising model system for future aggregation studies. Both mechanisms observed in the two cystatin model systems studied in the present work can lead to toxicity in diseases characterized by aggregates of misfolded proteins.

SUPPORTING INFORMATION AVAILABLE

Figures 1S−5S showing representative far-UV CD spectra of the constructs, reversibility of the thermal unfolding of MNEI and ORYZ, 1D ^{1}H NMR spectra of wild-type ORYZ and mutants, molecular models of MNEI, ORYZ, and two mutants, and thermal unfolding of four mutants of ORYZ. This material is available free of charge via the Internet at http://pubs.acs.org.

REFERENCES

1. Temussi, P. A., Masino, L., and Pastore, A. (2003) From Alzheimer to Huntington, why is a structural understanding so difficult? *EMBO J. 22*, 355–361.
2. Ross, C. A., and Poirier, M. A. (2005) Opinion, What is the role of protein aggregation in neurodegeneration? *Nat. Rev. Mol. Cell Biol. 6*, 891–898.
3. Ross, C. A., and Poirier, M. A. (2004) Protein aggregation and neurodegenerative disease. *Nat. Med. 10* (Suppl.), S10–S17.
4. Caughey, B., and Lansbury, P. T. (2003) Protofibrils pores fibrils and neurodegeneration, separating the responsible protein aggregates from the innocent bystanders. *Annu. Rev. Neurosci. 26*, 267–298.
5. Hardy, J., and Selkoe, D. J. (2002) The amyloid hypothesis of Alzheimer's disease, progress and problems on the road to therapeutics. *Science 297*, 353–356.
6. Bennett, M. J., Sawaya, M. R., and Eisenberg, D. (2006) Deposition diseases and 3D domain swapping. *Structure 14*, 811–824.
7. Gudmundsson, G., Hallgrímsson, J., Jónasson, T. A., and Bjarnason, O. (1972) Hereditary cerebral haemorrhage with amyloidosis. *Brain 95*, 387–404.
8. Abrahamson, M., and Grubb, A. (1994) Increased body temperature accelerates aggregation of the Leu-68−Gln mutant cystatin C, the amyloid-forming protein in hereditary cystatin C amyloid angiopathy. *Proc. Natl. Acad. Sci. U.S.A. 91*, 1416–1420.
9. Barrett, A. J. (1986) The cystatins: a diverse superfamily of cysteine peptidase inhibitors. *Biomed. Biochim. Acta 45*, 1363–1374.
10. Brown, W. M., and Dziegielewska, K. M. (1997) Friends and relations of the cystatin superfamily-new members and their evolution. *Protein Sci. 6*, 5–12.
11. Grubb, A. (2000) Cystatin C—properties and use as diagnostic marker. *Adv. Clin. Chem. 35*, 63–99.
12. Yamada, M. (2000) Cerebral amyloid angiopathy, an overview. *Neuropathology 20*, 8–22.
13. Janowski, R., Kozak, M., Jankowska, E., Grzonka, Z., Grubb, A., Abrahamson, M., and Jaskolski, M. (2001) Human cystatin C, an amyloidogenic protein, dimerizes through three-dimensional domain swapping. *Nat. Struct. Biol. 8*, 316–320.
14. Bennett, M. J., Choe, S., and Eisenberg, D. (1994) Refined structure of dimeric diphtheria toxin at 2 0 Å resolution. *Protein Sci. 3*, 1444–1463.
15. Konno, T. (2001) Multistep nucleus formation and a separate subunit contribution of the amyloidogenesis of heat-denatured monellin. *Protein Sci. 10*, 2093–2101.
16. Kim, S. H., Kang, C.-H., Kim, R., Cho, J. M., Lee, Y.-B., and Lee, T.-K. (1989) Redesigning a sweet protein, increased stability and renaturability. *Protein Eng. 2*, 571–575.
17. Jenko, S., Skarabot, M., Kenig, M., Guncar, G., Musevic, I., Turk, D., and Zerovnik, E. (2004) Different propensity to form amyloid fibrils by two homologous proteins—human stefins A and B: searching for an explanation. *Proteins 55*, 417–425.
18. Spadaccini, R., Crescenzi, O., Tancredi, T., De Casamassimi, N., Saviano, G., Scognamiglio, R., Di Donato, A., and Temussi, P. A. (2001) Solution structure of a sweet protein, nmr study of mnei, a single chain monellin. *J. Mol. Biol. 305*, 505–514.
19. Spadaccini, R., Trabucco, F., Saviano, G., Picone, D., Crescenzi, O., Tancredi, T., and Temussi, P. A. (2003) The mechanism of interaction of sweet proteins with the T1R2-T1R3 receptor, evidence from the solution structure of G16A-MNEI. *J. Mol. Biol. 328*, 683–692.
20. Morris, J. A., Martenson, R., Deibler, G., and Cagan, R. H. (1973) Characterization of monellin, a protein that tastes sweet. *J. Biol. Chem. 248*, 534–539.
21. Esposito, V., Gallucci, R., Picone, D., Tancredi, T., and Temussi, P. A. (2006) The importance of electrostatic potential in the interaction of sweet proteins with the sweet taste receptor. *J. Mol. Biol. 360*, 448–456.
22. Tancredi, T., Iijima, H., Saviano, G., Amodeo, P., and Temussi, P. A. (1992) Structural determination of the active site of a sweet protein: a ^{1}H NMR investigation of pMNEI. *FEBS Lett. 310*, 27–30.
23. Konno, T., Murata, K., and Nagayama, K. (1999) Amyloid-like aggregates of a plant protein, a case of a sweet-tasting protein monellin. *FEBS Lett. 454*, 122–126.
24. Becktel, W. J., and Schellman, J. A . (1987) Protein stability curves. *Biopolymers 26*, 1859–1877.
25. Masino, L., Martin, S. R., and Bayley, P. M. (2000) Ligand binding and thermodynamic stability of a multi-domain protein calmodulin. *Protein Sci. 9*, 1519–1529.
26. Myers, J. K., Pace, C. N., and Scholtz, J. M. (1995) Denaturant m values and heat capacity changes: relation to changes in accessible surface areas of protein unfolding. *Protein Sci. 4*, 2138–2148.
27. Levine, H. (1993) Thioflavine T interaction with synthetic Alzheimer's disease P3-amyloid peptides, detection of amyloid aggregation in solution. *Protein Sci. 2*, 404–410.
28. Naiki, H., Higuchi, K., Hosokawa, M., and Takeda, T. (1989) Fluorometric determination of amyloid fibrils in vitro using the fluorescent dye thioflavin T1. *Anal. Biochem. 177*, 244–249.
29. Temussi, P. A. (2002) Why are sweet proteins sweet? Interaction of brazzein, monellin and thaumatin with the T1R2-T1R3 receptor. *FEBS Lett. 526*, 1–4.
30. Thompson, J. D., Gibson, T. J., Plewniak, F., Jeanmougin, F., and Higgins, D. G. (1997) The CLUSTAL_X windows interface, flexible strategies for multiple sequence alignment aided by quality analysis tools. *Nucleic Acids Res. 24*, 4876–4882.
31. Abrahamson, M., Ritonja, A., Brown, M. A., Grubb, A., Machleidt, W., and Barrett, A. J. (1987) Identification of the probable inhibitory reactive sites of the cysteine proteinase inhibitors human cystatin C and chicken cystatin. *J. Biol. Chem. 262*, 9688–9694.
32. Nagata, K., Kudo, N., Abe, K., Arai, S., and Tanokura, M. (2000) Three-dimensional solution structure of oryzacystatin-I, a cysteine proteinase inhibitor of the rice *Oryza sativa* L. *japonica*. *Biochemistry 39*, 14753–14760.
33. Kenig, M., Jenko-Kokalj, S., Tusek-Znidaric, M., Pompe-Novak, M., Guncar, G., Turk, D., Waltho, J. P., Staniforth, R. A., Avbelj, F., and Zerovnik, E. (2006) Folding and amyloid-fibril formation for a series of human stefins' chimeras: any correlation? *Proteins 62*, 918–927.
34. Dobson, C. M. (2001) The structural basis of protein folding and its links with human disease. *Philos. Trans. R. Soc. London, Ser. B 356*, 133–145.
35. Nilsson, M., Wang, X., Rodziewicz-Motowidlo, S., Janowski, R., Lindström, V., Onnerfjord, P., Westermark, G, Grzonka, Z., Jaskolski, M., and Grubb, A. (2004) Prevention of domain swapping inhibits dimerization and amyloid fibril formation of cystatin C: use of engineered disulfide bridges, antibodies, and carboxymethylpapain to stabilize the monomeric form of cystatin C. *J. Biol. Chem. 279*, 24236–2445.
36. Janowski, R., Abrahamson, M., Grubb, A., and Jaskolski, M. (2004) Domain swapping in N-truncated human cystatin C. *J. Mol. Biol. 341*, 151–160.
37. Koradi, R., Billeter, M., and Wüthrich, K. (1996) MOLMOL: a program for display and analysis of macromolecular structure. *J. Mol. Graphics 14*, 51–55.